# Spacecraft Heat-Protection Requirements for Mars Aerodynamic Braking

G. M. HANLEY* AND F. J. LYON†
*North American Aviation, Inc., Downey, Calif.*

**The heat protection required for decelerating a spacecraft by aerodynamic braking to establish an orbit about the planet Mars is determined. The effect of vehicle shape on heat-protection weight at a nominal entry velocity of 27,600 fps and the effect of initial entry velocity on heat shielding of a selected configuration for entry velocities between 27,600 and 39,000 fps are studied. Effects of the wide spread in current estimates of the constituents and density of the Martian atmosphere are also evaluated. It is shown that gas radiation is a major source of gasdynamic heating during atmospheric braking, even for entry at 27,600 fps. Consequently, blunt shapes such as the Apollo configuration have higher heat-protection weight requirements than finer shapes such as the *M*-2 and high lift/drag ratio (*L*/*D*) Delta-Wing shapes. A modified conical vehicle having a half-cone angle of 18° and an $(L/D)_{max}$ = 1.16 was studied to determine the effect of initial entry velocity on vehicle heat-protection weight. The results of these studies indicate that Mars aerodynamic deceleration appears technically feasible and highly attractive when compared to the use of retrothrust for orbiting Mars.**

## Introduction

ONE of the most difficult operational problems associated with manned exploration missions to the planet Mars is efficiently accomplishing spacecraft or exploration module deceleration to effect orbital capture. Depending upon the Earth-Mars transit time, a spacecraft can be expected to approach Mars at hyperbolic velocities between around 20,000 and 40,000 fps. Because of the large propellant weight required to accomplish deceleration to orbital velocities with retrothrust, a potentially attractive technique is to fly through the Mars atmosphere in a manner sufficient to produce the required deceleration (braking by aerodynamic drag). The ob ective of this paper is to indicate heat-protection requirements associated with use of this technique for future manned Mars missions.

For the basic mission considered in this study, the Mars entry velocity is 27,600 fps. Although aerodynamic heating is not considered particularly severe under these conditions for manned Earth entry, no such assurance exists while entering the atmosphere of Mars, particularly in view of the large sizes and weights of an aerodynamic braking vehicle. As a consequence of this, it is desirable to review briefly the current state of the art regarding prediction of convective and radiant heating rates in the Mars atmosphere. In addition, the effect of the Mars atmosphere on vehicle aerodynamic characteristics is reviewed to determine whether any significant problems exist in the aerodynamic analysis of Mars entry vehicles.

Following brief descriptions of the anticipated Mars atmosphere and aerothermodynamic methods of analysis applicable in the Mars environment, entry trajectories are discussed, and parametric studies to identify the most attractive configuration for this mission are described. One vehicle configuration is then selected for further aerodynamic and thermodynamic analysis to establish the required heat-shield weight and to assess potential aerothermodynamic problem areas.

Presented as Preprint 64-14 at the 1st AIAA Annual Meeting, Washington, D. C., June 29–July 2, 1964; revision received November 9, 1964. This study was conducted for the NASA Manned Spacecraft Center under Contract No. NAS 9-1748.

* Supervisor, Flight Sciences Department, Space and Information Systems Division. Member AIAA.

† Chief, Flight Sciences Department, Space and Information Systems Division. Associate Fellow Member AIAA.

## Methods of Analysis

### Mars Atmosphere

In order to place this subject in the proper perspective, it must be recognized that a great deal of uncertainty still exists regarding the Earth's atmosphere at high altitudes, and only since the advent of artificial satellites has quantitative information been achieved regarding the large variations of temperature, pressure, and density which occur in the Earth's upper atmosphere as a function of time of day, season, and solar activity. Such uncertainties are greatly magnified when the atmosphere of Mars is considered, and have resulted in a very large number of so-called model atmospheres, with several orders-of-magnitude difference in recommended pressure and density profiles. A second common failing of these model atmospheres for Mars is the extension only to the stratosphere. The atmospheric models of Schilling[1] were selected for this study. Although the Schilling-Rand Model III atmosphere was selected as the single model most likely to be encountered, it was considered necessary to study both mean and extreme models; hence, the Schilling-Rand Model II atmospheres[1] were used up to 80 km. These atmospheres are based on a composition consisting of $N_2$ and $CO_2$, with traces of argon.

Very early in the study the necessity for atmospheric data for altitudes greater than 80 km became evident. Although the atmosphere of Mars is less dense at the surface than that of Earth by a factor of about 10, the lower gravitational acceleration of Mars produces equal densities at about 30 km. Above this altitude the atmosphere of Mars is more dense, and even at 200 km the atmosphere is aerodynamically dense in the sense that a vehicle would still experience continuum gasdynamics. Accordingly, extrapolations to 300 km were made (Fig. 1) for this study. Subsequent to this work, extrapolated data were published by Rand.[2] The recommended tentative minimum, tentative mean, and tentative maximum atmospheres of Ref. 2 are essentially the same up to 180 km as the lower-limit, mean, and upper-limit atmospheres utilized in this study, as shown in Fig. 1. Jet Propulsion Laboratory (JPL) investigators have recently proposed Mars model atmospheres that are significantly different from these; lower surface pressure and density and higher molecular weight are postulated due to higher concentrations of $CO_2$ and argon. The lowest-density JPL atmosphere ($W_2$) is indicated in Fig. 1.

### Gasdynamic Heating

*Convection:* Any differences between convective heating to a vehicle moving through the atmospheres of Earth and Mars at identical flight conditions are attributable to differences between the thermodynamic and transport properties of air and an $N_2$–$CO_2$ gas mixture. Since $N_2$ is the predominant species in each atmosphere, the major difference is the existence of $CO_2$ rather than $O_2$ in the Mars atmosphere. The effect of $CO_2$ concentration on laminar stagnation-point heating was investigated by Hoshizaki.[3] His results indicate that the effect of the different thermodynamic and transport properties of $CO_2$, as compared to air, causes only a 9% increase in heat-transfer rate. The comparison of Hoshizaki's results with experimental results obtained in shock tubes (Fig. 2) is inconclusive because of the scatter in experimental results. They do, however, tend to substantiate the conclusion that only a small increase in laminar stagnation-point heating rate might be expected in an atmosphere containing $CO_2$.

No such results have been obtained either experimentally or theoretically for turbulent heat transfer. Comparison of Eckert's reference enthalpy method for air[4] with results including the effects of dissociation[5] indicates that Eckert's method adequately predicts the effects of air dissociation. Because of the small increase in heat transfer found due to to the presence of $CO_2$ for laminar stagnation-point heating, Eckert's method was used for turbulent heat transfer in the Mars atmosphere. A local transition Reynolds number of 300,000 based on wetted distance was assumed.

*Radiation:* The effect of the percent of $CO_2$ in $N_2$ on the radiant intensity has been studied both theoretically and experimentally. Theoretical intensity variations were obtained by Spiegel,[6] and experimental variations in intensity were obtained by James.[7] A comparison[7] of these results (Fig. 3) indicates that the theoretical and experimental intensities are in fair agreement. For the lower velocity range, 16,400 to 21,300 fps, the intensity is seen to vary significantly with $CO_2$ concentration in an $N_2$–$CO_2$ mixture. For higher velocities, the effect of $CO_2$ concentration is seen to be of less importance Although the peak intensities are shown to be considerably higher than air in the velocity range shown, Spiegel's computations indicate that at higher velocities ($u_\infty \gtrsim 32{,}000$ fps) the intensity becomes independent of $CO_2$ concentration and is virtually identical to air intensity because of the similarity in important reactions. This trend has not yet been experimentally verified.

For the velocity range between 15,000 and 28,000 fps, Spiegel obtained the following approximate dependency of intensity on freestream density and velocity for a normal shock wave and a 7.5% $CO_2$ concentration:

$$I = 1.70 \times 10^{-11} \rho_\infty^{1.4} u_\infty^{5} \text{ (Btu/ft}^2\text{sec)} \qquad (1)$$

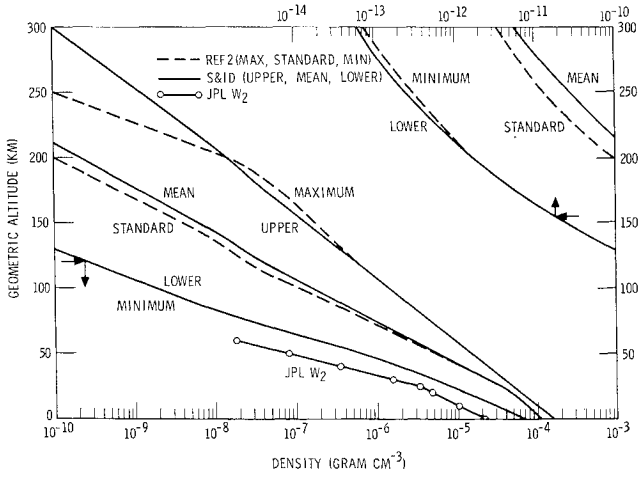


**Fig. 1 Mars model atmospheric densities.**

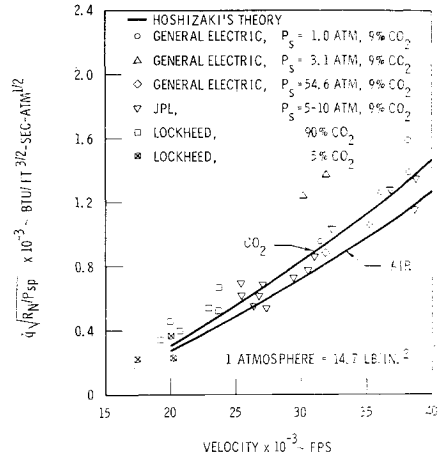


**Fig. 2 Comparison of stagnation-point convective heating theory and experimental data.**

Since the 7.5% $CO_2$ concentration intensities are near the maximum (Fig. 3), use of this relationship should give results near the highest possible. Because current estimates of the $CO_2$ concentration vary between 5 and 60% for the Mars atmosphere, use of a near-maximum value of intensity variation is justified.

At the higher velocities, the intensity variation for air is assumed to represent adequately the Mars radiant intensity. This variation is approximately given by

$$I = 7.8 \times 10^{-41} \rho_\infty^{1.8} u_\infty^{12} \text{ (Btu/ft}^2\text{sec)} \qquad (2)$$

for velocities in excess of 30,000 fps.[8] To insure conservatism in this study, the highest intensity of (1) or (2) is employed to establish the radiant intensity.

In the application of these equations to computation of the radiant heating rate to a vehicle, care must be taken to determine if the radiant heating rate to the vehicle is affected by absorption and/or energy decay within the shock layer, both of which tend to limit the possible radiant heating rate to the vehicle. Energy decay becomes important when the radiant heating rate is of the same order of magnitude as the freestream kinetic energy rate ($\rho_\infty u_\infty^3/2J$). Self-absorption becomes important when the radiant heating rate is of the same order of magnitude as black body radiation ($\sigma T_g^4$). For the conditions encountered by the aerodynamic braking vehicles in this study, energy decay in the shock layer was found to be of negligible importance. The radiant heating rates were, however, in the neighborhood of blackbody radiation when the infinite plane approximation for heating rate

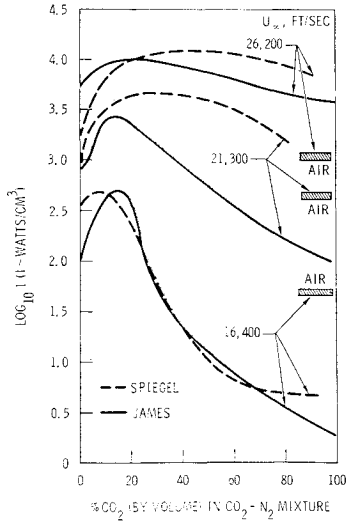


**Fig. 3 Comparison of experimental and theoretical radiant intensities for $CO_2$–$N_2$ mixtures.**

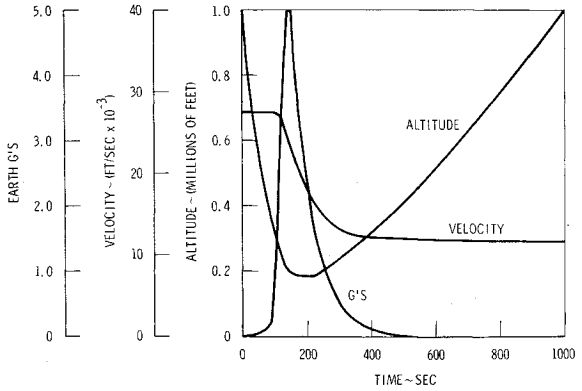


**Fig. 4 Apollo undershoot trajectory.**

was assumed, i.e., when $q = I\delta/2$, where $\delta$ is the shock standoff distance. Consequently, radiant heating rates were limited to include the effects of absorption using the results of Ref. 9.

### Aerodynamics

In addition to determining the effect of $CO_2$ concentration on radiant intensity, James and Smith[10] experimentally studied the effects of $CO_2$ concentration on static aerodynamic loads and stability. Their results indicate that, for both blunt and fine bodies at high Mach numbers, the force coefficients are nearly independent of $CO_2$ concentration and are virtually the same as those obtained using air. With the exception of configurations employing flares on the rear of the body, the static stability was also nearly independent of $CO_2$ concentration and was virtually identical to the same values obtained for air. Accordingly, it is sufficient to assume that test results of static aerodynamic coefficients available for air adequately represent the static coefficients for an aerodynamic braking vehicle in the Mars atmosphere, since flared bodies are not under consideration.

## Mars Entry Trajectories

Studies of Mars atmospheric trajectories were conducted under the assumption that all vehicles employ roll modulation for trajectory control during entry similar to the current Apollo Command Module control scheme. When this assumption is made, the vehicle ballistic coefficient ($W/C_DA$) is constant, assuming a constant wing loading and drag coefficient; and the vehicle $L/D$ ratio (with respect to the local vertical) is varied by rolling the vehicle about the velocity vector.

The entry corridor defined herein for Mars is bounded by the theoretical undershoot conic that gives a 5-$g$ maximum load factor during entry and the theoretical overshoot conic that reaches a pull-out altitude where the centrifugal acceleration is ust balanced by full negative lift and vehicle weight when full negative $L/D$ is employed during entry. Entry along the undershoot boundary is accomplished by employing full positive $L/D$ during the initial portion of entry, resulting in a maximum deceleration of 5 $g$ prior to pull-out (the position when the flight path angle becomes zero). Following pull-out, a constant altitude deceleration is maintained by roll-modulating $L/D$ to maintain a balance of forces in the radial direction until the velocity is somewhat above Mars circular velocity. The lift is then reduced to zero, and the vehicle exits from the atmosphere to an apoapsis altitude where orbit circularization is accomplished by using thrust. A 5-$g$ undershoot trajectory is shown in Fig. 4 for a vehicle with $L/D = 0.5$ and $W/C_DA = 414$ psf, typical of an Apollo-type aerodynamic braking vehicle. The initial entry velocity of 27,600 fps at $10^6$ ft altitude corresponds to the mission chosen for analysis. This figure indicates that the constant altitude deceleration at this entry velocity and for these vehicle parameters is brief, suggesting that a further increase in undershoot boundary deceleration followed by zero $L/D$ immediately at pull-out would probably result in too low a velocity for exit from the atmosphere.

For entry along the overshoot boundary, full negative $L/D$ is employed until pull-out. Beyond pull-out, the trajectory characteristics are similar to those described on the undershoot boundary. Detailed descriptions of Mars braking trajectories are given in Refs. 11 and 12.

## Vehicle Parametric Comparisons

During the initial phases of the study, three configurations were considered for aerothermodynamic analysis: the Apollo ($L/D = 0.5$), the $M$-2 ($L/D = 1.0$), and a Delta-Wing configuration ($L/D = 2.0$). The Apollo external shape is identical geometrically to the current Apollo Command Module. The $M$-2 shape consists basically of half of a 13.5° half-angle cone with a blunted nose. In planform, the Delta-Wing vehicle has a wing sweep angle of about 65°. The characteristics of these configurations are listed in Table 1. All of these vehicles were analyzed at an initial entry velocity (at an altitude of $10^6$ ft) of 27,600 fps. Gasdynamic heating and the resulting heat-shielding weights were computed at various locations on the vehicle for both overshoot and undershoot trajectories. The largest heat-shielding weight for undershoot and overshoot at each location was then employed to determine vehicle heat-shielding weight.

### Gasdynamic Heating

The gasdynamic heating rates to the three configurations were determined along the overshoot and 5-$g$ undershoot trajectories employing the methods of analysis previously described. Because of the large values of $W/C_DA$ for the vehicles, deceleration occurs at high values of freestream density, resulting in high Reynolds number and, consequently, turbulent flow over the major surface areas. In addition, high $W/C_DA$ and large physical dimensions lead to very significant radiant heating. The Apollo and $M$-2 vehicle heating rates at locations typical of the major surface areas are compared in Fig. 5 for flight along the 5-$g$ undershoot boundary. Because of gas radiation, the body shape plays an important role in the total heating to the vehicle. The radiant heating rate to the Apollo vehicle is much larger than the convective heating along the undershoot boundary; whereas, the radiant heating to the $M$-2 vehicle is small compared to the convective heating on the major areas of the vehicle.

### Heat-Shielding Materials

The criteria that were applied to select materials for heat shielding of the Mars braking vehicles were 1) that the materials be within the current state of the art as far as fabrication and knowledge of applicability is concerned, 2) that the materials have a proved heat-protection capability in heating environments similar to Mars, and 3) that the materials are capable of withstanding the high-vacuum and low-temperature conditions of space. A typical Apollo-

**Table 1 Aerodynamic parameters[a]**

| | Apollo | $M$-2 | Delta-Wing |
|---|---|---|---|
| $L/D$ | 0.5 | 1.0 | 2.0 |
| $\alpha$(deg) | 33 | 27 | 16 |
| $W/C_DA$ (psf) | 414 | 943 | 1980 |
| Signif. length (ft) | Diam, 38.2 | Length, 64.0 | Length, 56.6 |

[a] All vehicle volumes = 15,200 ft; all vehicle weights = 473, 800 lb.

type material was selected as the reference ablation material, because such materials have been thoroughly tested and qualified at hard-vacuum, low-temperature conditions. The heat-protection capability of this material in regions of high heat flux and for extended periods of time is proved. However, for regions of low heat flux, low-ablation-temperature materials such as Thermolag T-500 may prove superior to the Apollo-type material, and radiation cooling with a thin metallic external skin and internal insulation is also feasible. Therefore, the following heat-protection schemes were studied: 1) Apollo-type ablator on the entire vehicle, 2) Apollo-type ablator on the lower surface and in the stagnation regions and Thermolag T-500 on the upper surfaces, and 3) Apollo-type ablator on the lower surface and in the stagnation region and radiation cooling with Q-Felt insulation on the upper surfaces. Use of these three systems on the $M$-2 vehicle is compared in Fig. 6. The second (with Thermolag T-500 on the upper surface) yields highest weights for back-wall temperatures less than 900°R, and it cannot be used for back-wall temperatures above 960°R (its ablation temperature). The Q-Felt insulation with a columbium radiator on the upper surface gives the lowest heat-shield weight for all back-wall temperatures. In all cases, however, the differences in heat-shield weight are not significantly large. A similar trend was also noted when these concepts were compared on the Apollo and Delta-Wing configurations.

Since the Apollo-type material has been thoroughly ground-tested in hyperthermal environments and in the hard-vacuum, low-temperature environment that exists in space, its use over the entire vehicle appeared to be a reasonable approach for this study. However, since the Apollo-type material is a high-temperature charring ablator, the total mass loss during braking may not be as large as the mass losses of lower-temperature ablators such as Thermolag T-500. Unless the heat shield can be easily jettisoned following braking, the weight of the remaining heat shield must be included as a part of the vehicle weight for launch out of the Mars orbit for return to Earth. Under these conditions, even though a low-temperature ablator may be heavier prior to entry, it may be more effective than a high-temperature ablator from an over-all mission point of view.

For a purely convective thermal environment, it would be expected that the weight of the heat shield would increase with increasing $L/D$. Figure 6 shows that this trend holds between the M-2 and Delta-Wing vehicles. The Apollo vehicle, with an $L/D$ of only 0.5, has the greatest heat-protection weight (except at the higher back-wall temperatures) because it encounters severe radiant heating on nearly

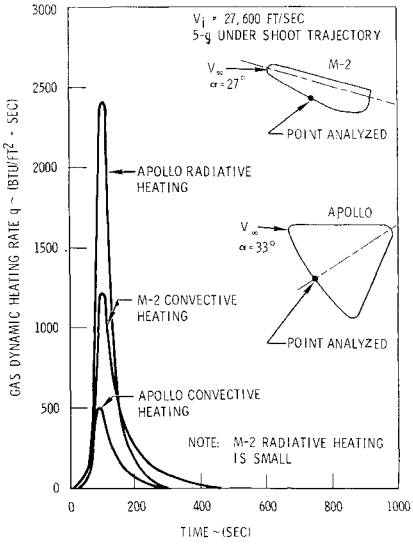


**Fig. 5 Apollo and $M$-2 heating rate comparison.**

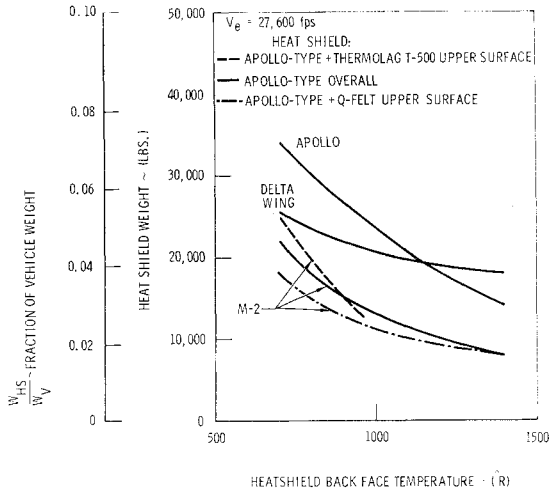


**Fig. 6 Comparison of heat-protection weights.**

its entire front, whereas the $M$-2 and Delta-Wing vehicles have only a small region that is significantly affected by radiant heating.

For current state-of-the-art bond-line temperatures of about 1000°R, Fig. 6 shows that the heat-protection system weight for the volume and total weight considered and for an entry velocity of 27,600 fps will range from about 2.8 to 5.0% of the vehicle weight.

The effective heat of ablation for the Apollo-type ablator is given by

$$q^* = 300 + 1.20\ \Delta H$$

where $\Delta H$ is the enthalpy difference across the boundary layer (Btu/lb). It was assumed in this study that the effective heats of ablation for radiation and convection are the same. During the time of peak heating, this effective heat of ablation was as high as 14,000 Btu/lb for the Apollo vehicle. Since it may be reasonable to expect that the effective heat of ablation for radiation is lower than the effective heat of ablation for convection, an estimate of the effect of holding the effective heat of ablation for radiation constant at 5000 Btu/lb was made. This resulted in a 22,000-lb weight increase for the Apollo vehicle, i.e., at a 1000°R back-wall temperature, the Apollo heat shield would weigh about 45,000 lb as compared to the 23,500 lb shown in Fig. 6.

### Parametric Vehicle Comparison Summary

The variation in heat-shield weight for the configurations studied is between 2.8 and 5.0% of the vehicle weight when entry is made at 27,600 fps. These weights may be compared with a retrothrust propellant requirement of 240% of the vehicle weight in Mars circular orbit at this velocity (for an $I_{SP}$ of 400 sec) if aerodynamic braking is not employed. The effect of this heat-protection system weight on total vehicle weight depends upon the ability to jettison the heat shield prior to initiating the transfer trajectory from Mars to Earth. The $M$-2 vehicle has the lowest heat-shield weight. The Apollo vehicle experiences predominantly radiant heating that causes a significant increase in heat-shield weight compared to the other configurations. At higher entry velocities it is expected that this trend will indicate even larger increases in the Apollo heat-shielding weight compared to the other vehicles. Radiant heating is less on a relatively fine shape both because of the smaller shock standoff distance (reducing the radiant heating rate) and the reduced area of the stagnation region.

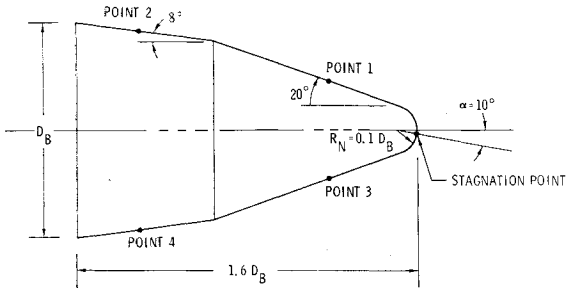


**Fig. 7 Configuration selected for detailed analysis.**

## Analysis of the Selected Configuration

As an outgrowth of these initial configuration studies and practical constraints due to integration with the entire spacecraft vehicle, one configuration possessing favorable aerothermodynamic characteristics was selected for further analysis. Booster compatibility considerations indicated that a symmetrical configuration was desirable, and Mars Excursion Module studies, conducted separately, indicated the desirability of a half-cone configuration. The configuration selected was a modified cone and is illustrated in Fig. 7. The objectives of further studies were to evaluate this vehicle's aerodynamic characteristics, to determine the sensitivity of heat-shield weight to entry velocity and atmospheric uncertainties, and to expose potential aerothermodynamic problem areas.

### Aerodynamics

Aerodynamic forces and moments for the selected configuration were computed using Newtonian flow analyses. The resulting lift and drag coefficients $C_L$ and $C_D$ and $L/D$ are presented as a function of angle of attack ($\alpha$) in Fig. 8. This figure indicates that a maximum $L/D$ of 1.16 occurs at $\alpha = 15°$; however, as explained in the following section, it was decided to restrict $\alpha$ to 10°, resulting in an $L/D$ of about 1.1. The Newtonian flow center of pressure (c.p.) for this configuration at $\alpha = 10°$ is located at 57% of the vehicle length measured from the nose along the centerline and appears to be farther forward than realistic center-of-gravity positions. The reason for the forward c.p. location is the large forward cone angle as compared to the aft cone angle on the configuration, coupled with a low $\alpha$. Wind-tunnel tests of similar configurations (cone-cylinders with higher fineness ratios)[13] indicate that c.p. is farther back than Newtonian theory predicts. Thus, a more detailed analysis of the aerodynamics of this type of configuration is required to establish firmly the longitudinal c.p. location. Moreover, no aerothermodynamic optimization of the nose radius was accomplished.

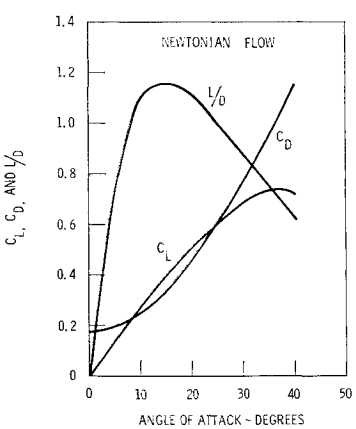


**Fig. 8 Selected configuration aerodynamic coefficients.**

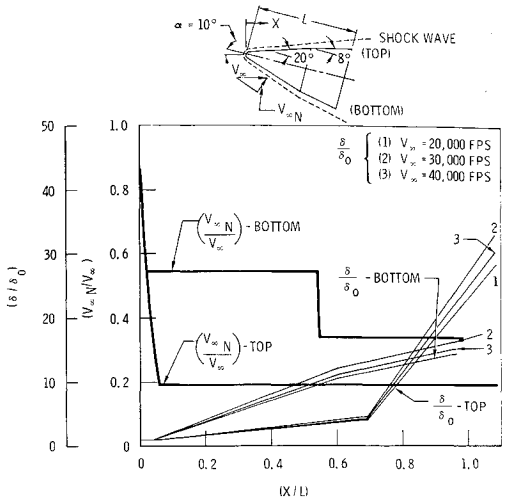


**Fig. 9 Variation of nondimensionalized velocity ratio and shock-detachment distance along modified cone configuration.**

### Effect of Angle of Attack on Heating

The effect of $\alpha$ on radiant heating to the lower side of the forward 20° cone was investigated. This region was selected because it represents a sizeable area of heat protection for the vehicle and because the radiant heating to this region is higher than the radiant heating to any other conic section of the vehicle. The major concern was that the radiant heating to this region of the vehicle may be significant, even at low $\alpha$, for entry at high velocities. Radiative heating rates were computed at a freestream velocity of 34,000 fps and a 5-$g$ condition, corresponding to the maximum $g$ condition for about a 38,000 fps initial entry velocity. The wing loading of the vehicle was assumed to be 524 psf, or, equivalently, a vehicle weight of 447,200 lb was assumed with a base diameter of 396 in. The corresponding values of $L/D$ and $W/C_DA$ are shown in Table 2, along with the corresponding freestream density for a 5-$g$ condition at 34,000 fps. The shock angle ($\theta$) shown in Table 3 was obtained by assuming that the local shock angle corresponds to the shock angle for a cone having a half-angle equal to the geometrical cone half-angle plus the angle of attack. From this, the local shock standoff distance was obtained, and the corresponding radiant heating rate was computed using Eq. (1) for the intensity variation, where $u_\infty$ is replaced by the velocity component normal to the shock wave. The radiant heating was then computed assuming an infinite plane radiating geometry. The results of this computation were compared with blackbody heating rates for the equilibrium gas temperature immediately behind the oblique shock wave, and it was determined that the heating rates were all in the neighborhood of blackbody heating rates at this location. The temperatures behind the oblique shock wave and the blackbody heating rates are shown in Table 3 as a function of $\alpha$, along with the heating values obtained assuming an infinite plane radiating geometry. These results indicate that under the specified conditions radiant heating represents a significant heating contribution to the lower portion of the forward cone. Under these same conditions, the turbulent convective heating rates are between approximately 4500 and 5100 Btu/ft²-sec. As a

**Table 2 Effect of angle of attack on configuration characteristics**

| $\alpha$ (deg) | 10 | 15 | 20 |
|---|---|---|---|
| $L/D$ | 1.09 | 1.16 | 1.12 |
| $W/C_DA$ (lb/ft²) | 2100 | 1530 | 1145 |
| $\rho_\infty \times 10^5$ (slugs/ft³) | 1.23 | 0.86 | 0.66 |

result, it was decided that $\alpha = 10°$ should be employed during entry to reduce the radiant heating problem although still maintaining $L/D \simeq 1.1$.

The preceding results are not intended to indicate an optimum $\alpha$ during Mars braking. In order to determine the "optimum" $\alpha$, it would be necessary to examine the vehicle trajectories, the resulting heating rates around the vehicle, and the effect of these heating rates on heat-protection weight. At lower entry velocities (for example 28,000 fps) it is not anticipated that radiant heating will pose nearly as severe a problem as indicated previously. As a consequence, use of $\alpha > 10°$ during entry at low velocities may reduce the total heat-protection weight.

### Effect of Velocity on Heating

An $\alpha$ of 10° during entry was assumed for thermal analysis at the configuration locations shown in Fig. 7. Convective and radiative heating rates were computed for the nominal atmosphere for entry velocities between 27,600 and 39,000 fps and for the extreme atmospheres at an entry velocity of 34,400 fps. Radiative heating rates at these locations were computed using the highest of the intensity variations given by Eqs. (1) and (2) and with the assumption of an isothermal infinite radiating plane at points 1, 2, 3, and 4 and an isothermal spherical radiating geometry at the stagnation point. The effect of self-absorption of the gas[9] was included. The local shock angle was computed in the pitch plane assuming an equivalent tangent cone, where the cone half-angle is the local angle of attack relative to the freestream velocity vector. The local shock standoff distance ($\delta$) is assumed constant at the stagnation value for the hemispherical nose region ($\delta/\delta_0 = 1 = \text{const}$) and was assumed to increase linearly from the point where the bow shock joins the conical shocks. Figure 9 indicates large $\delta/\delta_0$ for points along the conic sections of the vehicle. In particular, at point 3 this standoff distance coupled with a large shock angle tends to give significant radiative heating at the high entry velocities.

It should be noted that the assumptions made regarding shock geometry are considerably simplified and may lead to nonconservative results because of the following factors: 1) $\delta/\delta_0$ is not actually constant on the hemispherical nose (it increases away from the stagnation point around a spherical geometry); 2) an almost two-dimensional Prandtl-Meyer expansion would exist at the conical intersections, rather than the assumed sudden change in shock angle; and 3) as a result of the blunt nose, a region of high-enthalpy gas would exist near the body (it was assumed that the temperature of the gas in the conical regions depended only on local shock angle). Each of these simplifications tends to give nonconservative results.

Comparisons of the convective and radiative stagnation-point heating rate time history along the overshoot boundary for the low- and high-entry-velocity cases with the nominal atmosphere are shown in Fig. 10. Radiant heating is dominant in the stagnation region for the entire velocity range investigated. The ratio of peak radiative to peak convective heating rate is about 3 at 27,600 fps and increases to about 12 at 39,000 fps. The total stagnation-point convective and radiative heating integrated over the time from initial entry to atmospheric exit is shown in Fig. 11. Because of the higher power dependency on velocity of radiation heating rate, the ratios of radiative to convective integrated heating are not as large as the ratios of the peak values.

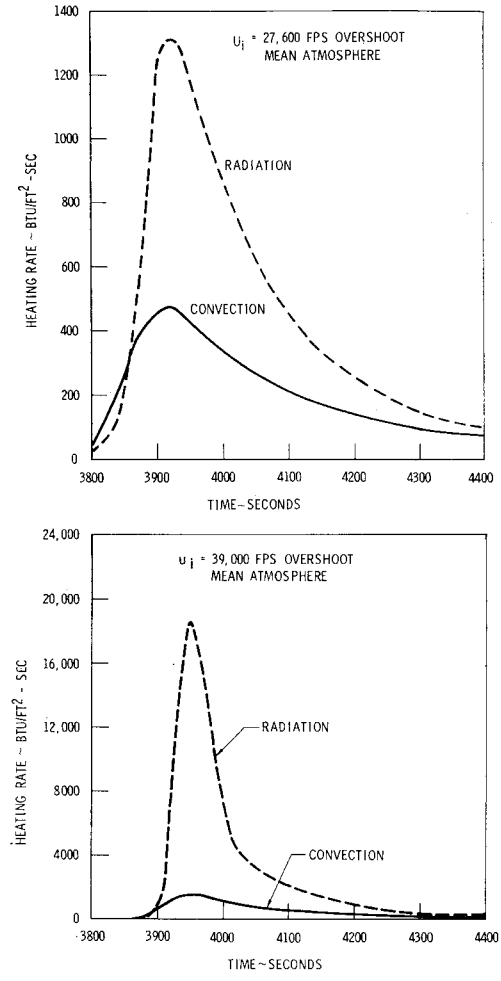


**Fig. 10 Stagnation-point heating rate.**

### Effect of Atmospheric Properties

In addition to investigating aerodynamic heating for the nominal Mars atmosphere, entries into the atmospheres representing the high and low Schilling[2] extremes of density were studied to determine the effects of these atmospheres on heat-protection requirements. Integrated convective and radiative heating rates ($Q_C$ and $Q_R$, respectively) for various points on the vehicle are shown in Table 4 for an initial entry velocity of 34,400 fps along the overshoot boundary. The results indicate that the effect of the atmospheric density profile on integrated radiant and convective heating is negligible. Furthermore, the differences in time of flight are

**Table 3 Effect of angle of attack on radiative heating rates**

| $\alpha$ (deg) | 10 | 15 | 20 |
|---|---|---|---|
| Shock angle, $\theta$ (deg) | 33.2 | 38.8 | 44.8 |
| Temperature behind shock (°R) | 11,900 | 12,800 | 13,500 |
| Blackbody heating (Btu/ft$^2$ sec) | 9,460 | 12,800 | 15,800 |
| Infinite plane heating (Btu/ft$^2$ sec) | 8,650 | 12,000 | 19,100 |

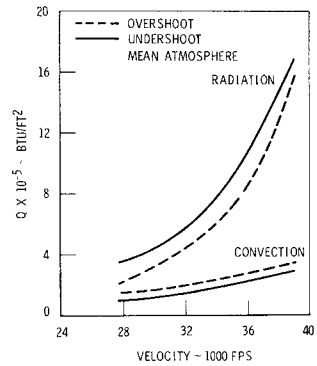


**Fig. 11 Total stagnation-point heating.**

**Table 4 Effect of atmosphere on total heating, $10^3$ Btu/ft$^2$ (entry velocity = 34,400 fps, overshoot boundary)**

| Atmosphere | Flight time (sec) | Pt. 1 | | Pt. 2 | | Pt. 3 | | Pt. 4 | |
|---|---|---|---|---|---|---|---|---|---|
| | | $Q_C$ | $Q_R$ | $Q_C$ | $Q_R$ | $Q_C$ | $Q_R$ | $Q_C$ | $Q_R$ |
| Lower | 1940 | 132 | Neg. | 5.06 | 2.45 | 620 | 159 | 270 | 39.0 |
| Mean | 1790 | 133 | Neg. | 5.53 | 2.44 | 622 | 158 | 275 | 38.8 |
| Upper | 1680 | 135 | Neg. | 5.74 | 2.36 | 630 | 154 | 276 | 37.6 |

primarily due to the shorter time (for the high-density atmosphere) and the longer time (for the low-density atmosphere) required to reach the same atmospheric density when flight between an arbitrarily defined entry and exit altitude of $10_6$ ft is considered. However, it should be noted that the 7.5% $CO_2$ concentration was assumed in computing the radiant heating rates, and that a variation in $CO_2$ concentration would significantly alter the radiant heating rates. However, at the low entry velocities where large variations in radiant intensity exist with $CO_2$ concentration, the effect of radiant heating on heat-shield weight is diminished, and, consequently, the $CO_2$ variation may not seriously affect heat-shielding weight. If argon is found to be present in large quantities, however, a significant increase in high-velocity radiant heating would probably occur.

### Heat-Shielding Analysis

The points on the selected configuration shown in Fig. 7 were analyzed to determine heat-protection requirements as a function of heat-shield back-face temperature. The heat-protection material assumed was an ablator like that currently employed on the Apollo Command Module. In addition, it is assumed that a minimum-gage titanium skin is bonded to the exterior of the ablator to afford protection from the space environment during Earth-Mars transit. This thin skin has little significance in the Mars braking aerothermodynamic analysis, since it would be consumed early in entry over most portions of the vehicle. Two important functions are served by the skin: 1) a retention of material volatiles by protecting against the hard vacuum and 2) an aid in avoiding heat-shield fragmentation due to micrometeoroid impact. Titanium was selected rather than aluminum because of aerodynamic heating of the skin during Earth launch.

The gasdynamic heating conditions imposed during entry along the overshoot and undershoot trajectories were compared at each vehicle point, and the heat shield was designed to sustain the worst condition. Heat-protection weights were computed as functions of heat-shield back-face temperature for the nominal and extreme atmospheres. The weight variations with velocity and back-wall temperature are shown in Fig. 12, which indicates that heat-protection weight increases rapidly with velocity. This rapid increase is due in part to the increasing importance of radiative heating with velocity. For the 760°R back-wall temperature and the assumed total vehicle weight of 447,200 lb the heat-shield weight is 7.7% of the vehicle weight at a 27,000 fps entry velocity and 20.1% at 39,000 fps. These percentages cannot be directly compared to those previously obtained in the vehicle comparison study, because the vehicle volume is 26,000 ft$^3$ as compared to 15,200 ft$^3$ for the previous comparison vehicles.

The variation of temperature through the ablator and substructure was computed on the lower aft portion of the vehicle at 27,600 fps for entry along the overshoot boundary. A typical section through the vehicle is shown in Fig. 13. The external layer consists of Apollo-type ablation material bonded to a titanium or aluminum skin with a phenolic laminate core filled with Fiberglas for meteoroid protection. The structure consists of an Al or Ti sandwich with a phenolic laminate honeycomb. The temperature histories for the indicated locations with an ablator thickness of 1.5 in. are shown in Fig. 13. The $g$-load history indicates the imposed loading conditions. In both cases, the structural temperature has not significantly changed from the initial temperature when peak $g$'s occur. Peak temperatures occur under virtually a zero-$g$ condition. Figure 14 indicates that the ablator thickness significantly affects the temperature at the back-wall of the ablator, but the temperature at the back-face of the honeycomb structure is hardly affected.

The heat-shielding weights presented previously have been computed under many restrictive assumptions. The most important of these assumptions is that the heat of ablation of the Apollo-type ablation material employed for heat protection is similar to that currently employed for the Apollo Command Module; and furthermore, no modification to this effective heat of ablation was made for radiant heating. As a result of the existence of turbulent flow, a lower effective heat of ablation might be expected. Moreover, the high surface shearing stresses will also tend to re-

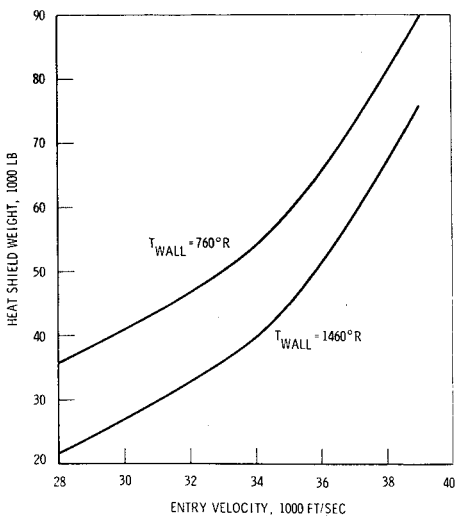


**Fig. 12 Effect of entry velocity on selected configuration heat-shield weight.**

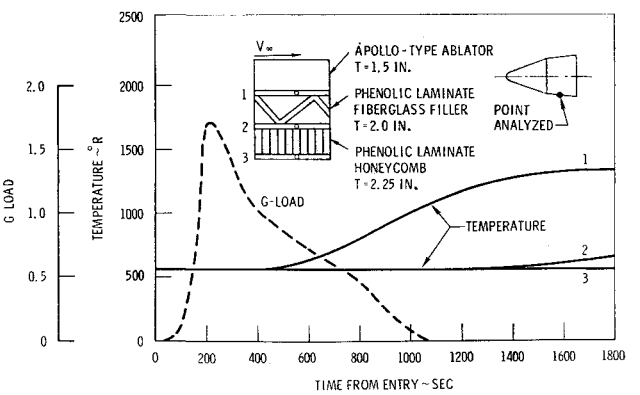


**Fig. 13 Structural temperature variation overshoot entry ($Ve$ = 27,600 fps).**

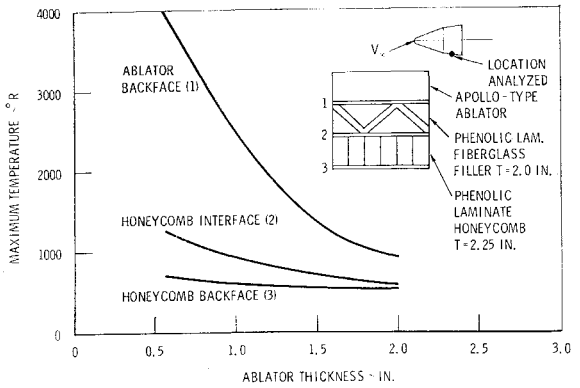


**Fig. 14 Ablator thickness variation, overshoot entry ($Ve$ = 27,600 fps).**

move surface material, possibly resulting in even less efficient ablation heat protection. The atmospheric constituents play an important role in the loss of heat-shielding material by surface chemical reactions. These reactions may be significantly different for the Mars atmosphere as compared to air. A more detailed study of the effectiveness of ablators in the turbulent high-shear and radiant Mars atmospheric environment is required to define further the heat-protection capability of candidate materials.

## Conclusions

The following conclusions can be made regarding the heating of spacecraft during aerodynamic braking at Mars: 1) radiant heating constitutes a significant portion of total heating at high entry velocities, resulting in large heat-shield weights for blunt configurations such as Apollo; 2) although radiation intensity depends strongly on the $CO_2$ content of the Martian atmosphere at low entry velocities, with maximum intensity occurring near 10% $CO_2$ concentration, the sensitivity of radiant heating (and thus heat-shield weight) to $CO_2$ concentration at the higher entry velocities where radiant heating is predominant is relatively small; 3) the effect of atmospheric density extremes on heat-protection weight is negligible; and 4) heat-shield weights for the configuration and mission considered in this paper vary from about 8 to 20% of total vehicle weight at entry velocities between 27,600 and 39,000 fps.

This study has shown that aerodynamic braking of Mars exploration vehicles is not only feasible but highly attractive when compared with retrothrust braking on a total system weight basis. Obviously, additional studies of specific missions and configurations involving more technical depth are required. In particular, a more concentrated study of the detailed heat-shield chemical and mechanical erosion processes during Mars entry is necessary to evaluate adequately specific heat-protection system weights.

## References

[1] Schilling, G. F., "Limiting model atmosphere of Mars," Rand Corp. Rept. RAND-R-402 (August 1962).

[2] Schilling, G. F., "Parametric limits for the upper atmosphere of Mars," Rand Corp. Rept. RAND-RM-3885-PR (November 1963).

[3] Hoshizaki, H., "Heat transfer in planetary atmospheres at super-satellite speed," ARS J. **32**, 1544–1551 (1962).

[4] Eckert, E. R. G., "Survey on heat transfer at high speeds," Wright Air Development Center TR 54-70, U. S. Air Force (1954).

[5] Dorrance, W. H., "Dissociation effects upon compressible turbulent boundary layer skin friction and heat transfer," ARS J. **31**, 61–70 (1961).

[6] Spiegel, J. M., Wolf, F., and Horton, T., "Aerothermodynamics of planetary entry," Jet Propulsion Lab., Solar Probe Spacecraft Rept. SPS37-22, Vol. IV, Sec. 354 (August 31, 1963).

[7] James, C. S., "Experimental study of radiative transport from hot gases simulating in composition the atmospheres of Mars and Venus," AIAA Preprint 63-455 (1963).

[8] McRae, W. V., "First quarterly report, manned Mars landing and return mission study," Contract NAS-2-1408, North American Aviation, Inc., Space and Information Systems Div. Rept. SID 63-1129 (1963).

[9] Koh, J. C. Y., "Radiation from nonisothermal gases to the stagnation point of a hypersonic blunt body," ARS J. **32**, 1374–1377 (1962).

[10] James, C. S. and Smith, W. G., "Experimental studies of static stability and radiative heating associated with Mars and Venus entry," IAS Paper FF-34 (1963).

[11] Napolin, A. L. and Mendez, J. C., "Target orbit selection for Mars missions using aerodynamic maneuvering," AIAA Preprint 64-14 (1964).

[12] Finch, T. W., "Aerodynamic braking trajectories for planetary orbit attainment," AIAA Preprint 64-478 (1964).

[13] Dennis, D. H. and Cunningham, V. E., "Forces and moments on inclined bodies at Mach numbers from 3.0 to 6.3," NASA-RM-A54EO3 (1954).